Supporting Information

Efficient doped and non-doped OLED based on a deep-blue HLCT material and all-HLCT WOLED with standard white-light emission

Xiaotian Chen[a], Hui Dai[a], Xu Zhang[a], Gaoyu Li[a, *], Zhiyong Yang[a, *], Juan Zhao[b, *], Zhenguo Chi[b, *]

[a] *Guangdong Engineering Technology Research Center for High-performance Organic and Polymer Photoelectric Functional Films, State Key Laboratory of Optoelectronic Material and Technologies, School of Chemistry, Sun Yat-sen University, Guangzhou, China*

[b] *School of Environmental and Chemical Engineering, Wuyi University, Jiangmen, 529020, China*

E-mail address: zhaoj95@wyu.edu.cn (J. Zhao); ligy69@mail.sysu.edu.cn (G. Li); yangzhy29@mail.sysu.edu.cn (Z. Yang); chizhg@mail.sysu.edu.cn (Z. Chi)

Contents

S1 Synthesis and Characterization

All pharmaceuticals and reagents used for synthesis can be readily purchased. Among them, (4-(9H-carbazol-9-yl)phenyl)boronic acid, 1,6-dibromopyrene, 4-bromo-N-(4-bromophenyl)-N-phenylaniline, (4-(diphenylamino)phenyl)boronic acid and 4,7-bis(4,4,5,5-tetramethyl-1,3,2-dioxaborolan-2-yl)benzo[c][1,2,5]thiadiazole are all from Shanghai Aladdin Biochemical Technology Co., Ltd, 1-phenyl-2-(4-(4,4,5,5-tetramethyl-1,3,2-dioxaborolan-2-yl)phenyl)-1H-phenanthro[9,10-d] imidazole is from Suzhou Gekai Optical New Material Co., Ltd.

^{1}H NMR and were ^{13}C NMR recorded on a Bruker ADVANCE III 400 /600 spectrometer in dimethyl sulfoxide d_6 (DMSO-d_6) at room temperature (except for compounds CzPyBr and BTPA4 which dissolved in Methylene Chloride-d_2), with tetramethylsilane (TMS, $\delta = 0$) as the internal standard. High resolution mass spectra (HRMS) were measured on a Bruker ultrafle Xtreme mass spectrometer operating in MALDI-TOF mode.

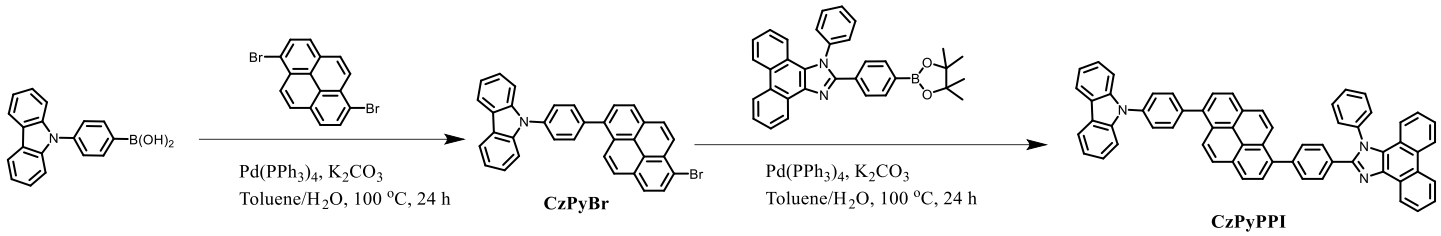

Scheme S1. Molecular structures and synthetic routes of the CzPyPPI.

Synthesis of 9-(4-(6-bromopyren-1-yl) phenyl)-9H-carbazole (CzPyBr)

The synthesis of the key intermediate 9-(4-(6-bromopyren-1-yl) phenyl)-9H-carbazole (CzPyBr) followed a similar procedure as reported by Kim et al. (Chem. Eng. J. 2025, 166658) with slight modifications. At room temperature, (4-(9H-carbazol-9-yl)phenyl)boronic acid (2.00 g，6.97 mmol), and 1,6-dibromopyrene (2.51 g, 6.97 mmol) were added to a 250 mL three-necked flask and dissolved in 100 mL of toluene. The mixture was stirred for 30 min under an argon atmosphere, then 15 mL of a 0.34 mol/L aqueous solution of K_2CO_3 and 0.05 g of Pd $(PPh_3)_4$ were added. The temperature was raised to 100°C and the reaction was stirred for 24 h. After the reaction was completed, the mixture was cooled to room temperature, the solvent was removed by vacuum distillation, and the product was purified by column chromatography (DCM/nH = 1:4 v/v) to obtain a white powder solid (1.56 g, yield 42.9%). ^{1}H NMR (400 MHz, Methylene Chloride-d_2) δ 8.53 (d, J = 9.2 Hz, 1H), 8.35 (d, J = 8.2 Hz, 1H), 8.26 – 8.19 (m, 2H), 8.12 (d, J = 7.8 Hz, 5H), 7.51 (d, J = 8.1 Hz, 4H), 7.48 - 7.44 (m, 3H), 7.27 (t, J = 7.4 Hz, 4H).

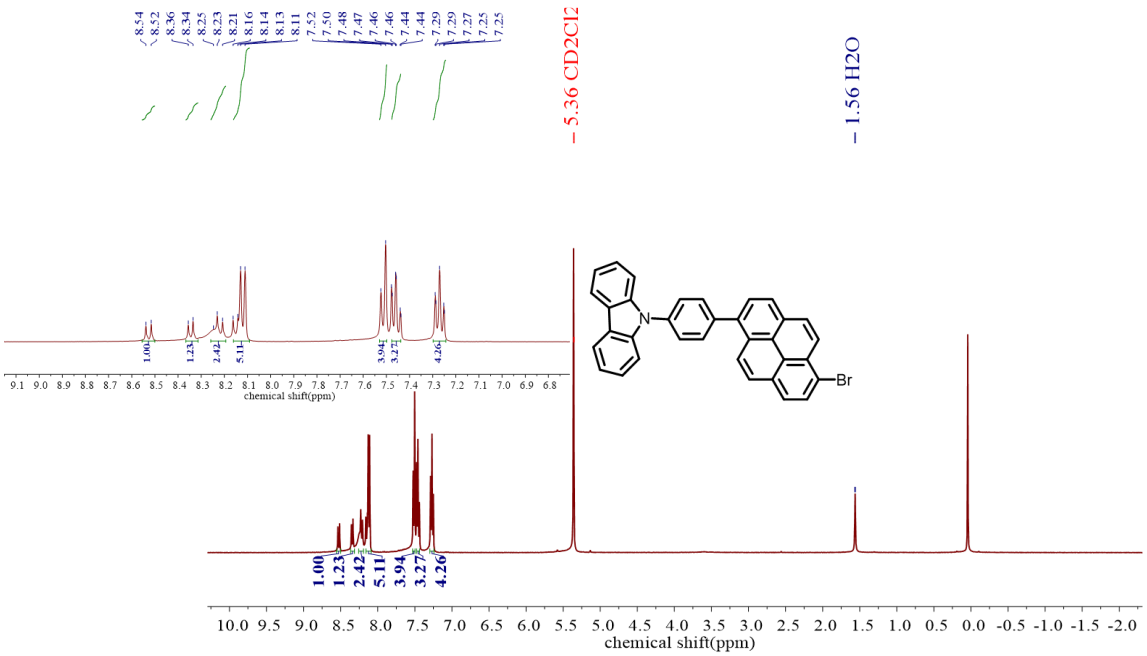

Figure S1. ^{1}H NMR spectrum of CzPyBr in Methylene Chloride-d_2.

Synthesis of 2-(4-(6-(4-(9H-carbazol-9-yl) phenyl) pyren-1-yl) phenyl)-1-phenyl-1H-phenanthro[9,10-d] imidazole (CzPyPPI)

At room temperature, CzPyBr (0.99 g，1.89 mmol) and 1-phenyl-2-(4-(4,4,5,5-tetramethyl-1,3,2-dioxaborolan-2-yl)phenyl)-1H-phenanthro[9,10-d]imidazole (0.94 g, 1.89 mmol) were added to a 250 mL three-necked flask and dissolved in 100 mL of toluene. The mixture was stirred for 30 min under an argon atmosphere, then 15 mL of a 0.34 mol/L aqueous solution of K_2CO_3 and 0.05 g of Pd $(PPh_3)_4$ were added. The temperature was raised to 100°C and the reaction was stirred for 24 h. After the reaction was completed, the mixture was cooled to room temperature, the solvent was removed by vacuum distillation, and the product was purified by column chromatography (DCM/nH = 1:1 v/v) to obtain a light pale-yellow powder solid (0.46 g, yield 29.9%). ^{1}H NMR (400 MHz, DMSO-d_6) δ 8.98 (d, J = 8.5 Hz, 1H), 8.93 (d, J = 8.4 Hz, 1H), 8.78 (d, J = 8.0 Hz, 2H), 8.51-8.41 (m, 3H), 8.40-8.27 (m, 5H), 8.22 (d, J = 7.8 Hz, 1H), 8.16 (d, J = 9.3 Hz, 1H), 8.08 (d, J = 7.8 Hz, 1H), 7.98 (d, J = 8.0 Hz, 3H), 7.95-7.84 (m, 6H), 7.84-7.78 (m, 3H), 7.74 (t, J = 7.7 Hz, 1H), 7.68 (d, J = 8.0 Hz, 1H), 7.64 (d, J = 8.2 Hz, 2H), 7.59 (d, J = 7.8 Hz, 1H), 7.52 (d, J

= 7.9 Hz, 1H), 7.37 (q, J = 8.2, 7.7 Hz, 3H), 7.14 (d, J = 8.2 Hz, 1H). ^{13}C NMR (600 MHz, DMSO-d_6) δ 151.04, 138.64, 136.92, 130.78, 130.73, 130.68, 129.64, 129.60, 129.46, 128.97, 128.67, 128.14, 127.94, 127.10, 126.21, 125.68, 124.98, 124.15, 122.96, 122.47, 120.65, 40.63, 40.42, 40.21, 40.00, 39.79, 39.58, 39.37. HRMS (APCI): m/z, $[M+H]^+$ calcd for $C_{61}H_{37}N_3$: 812.30602, found: 812.30603.

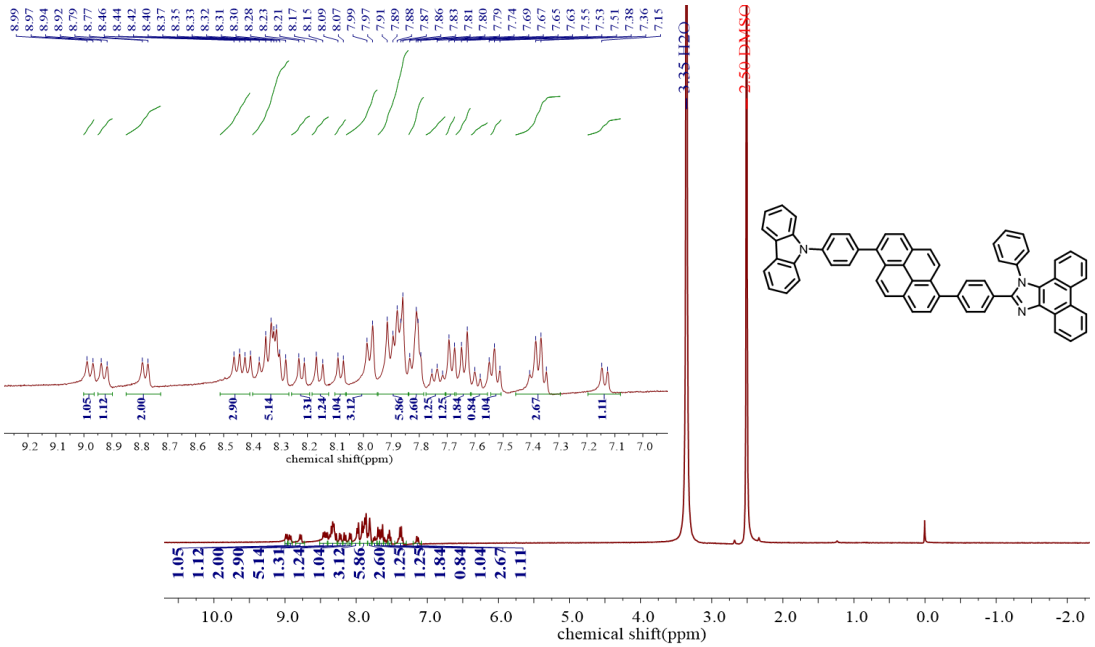

Figure S2. ^{1}H NMR spectrum of CzPyPPI in DMSO-d_6.

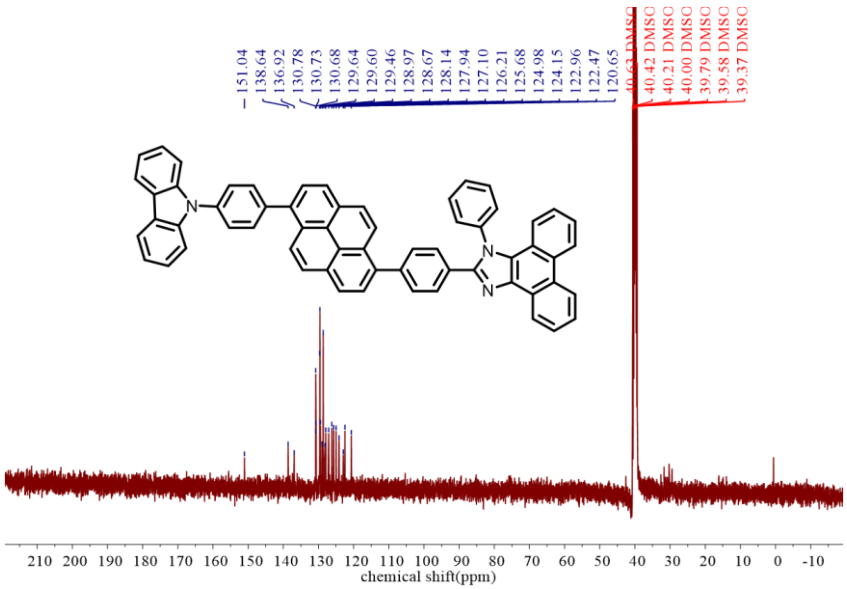

Figure S3. ^{13}C NMR spectrum of CzPyPPI in DMSO-d_6.

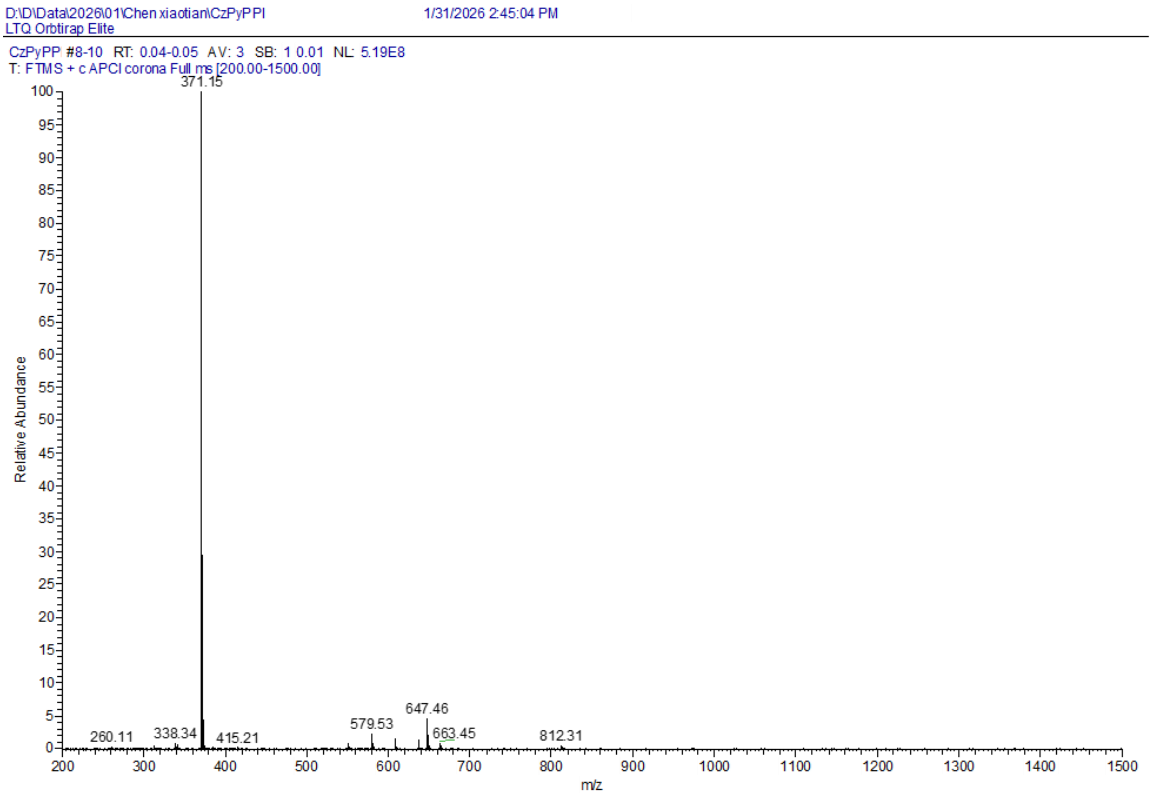

Figure S4. HRMS spectrum of the CzPyPPI (full-range).

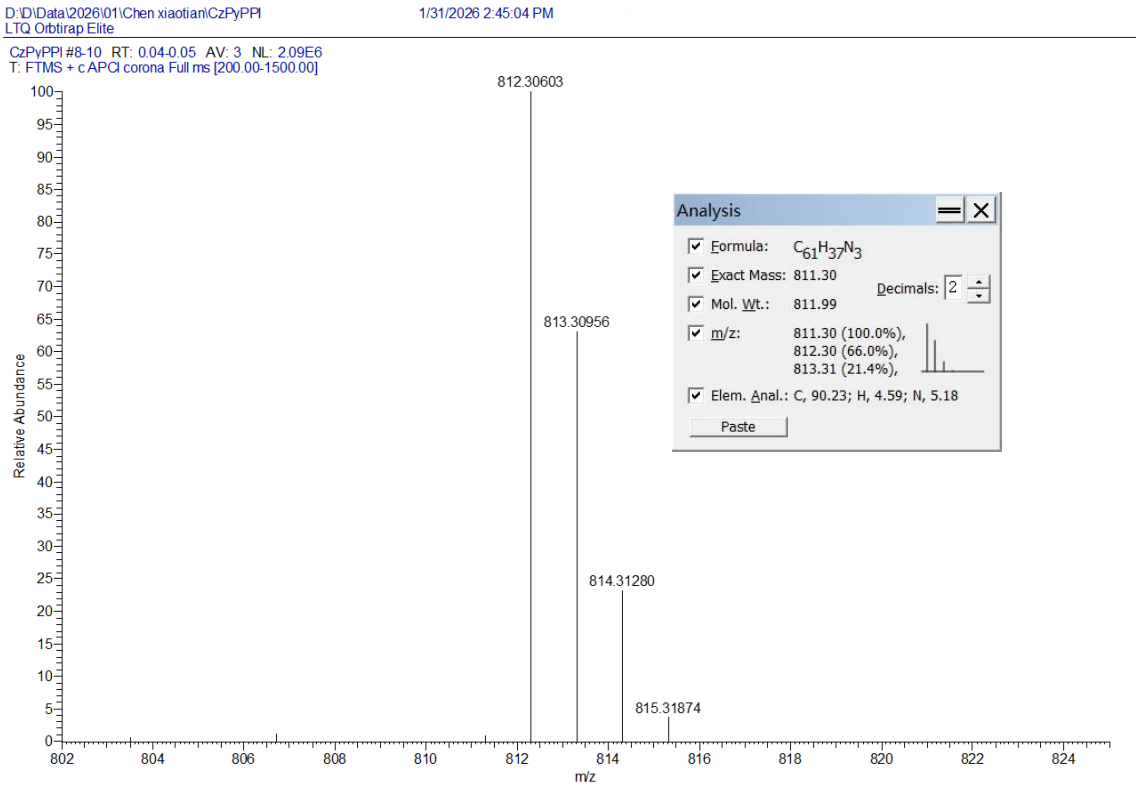

Figure S5. HRMS spectrum of the CzPyPPI.

Fragmentation assignment for CzPyPPI: The full-range HRMS spectrum of CzPyPPI (Figure S4) shows two dominant peaks. The highest peak at m/z ≈ 371 is assigned to the phenanthroimidazole (PPI) unit, which is a stable fragment formed by cleavage of the bond connecting the PPI moiety to the pyrene core. The second highest peak at m/z ≈ 647 corresponds to the molecule after loss of the carbazole unit. The exact mass of the molecular ion peak $[M+H]^+$ (calculated for CzPyPPI) is clearly detectable with a mass error of < 3 ppm, (Figure S5) confirming the molecular formula.

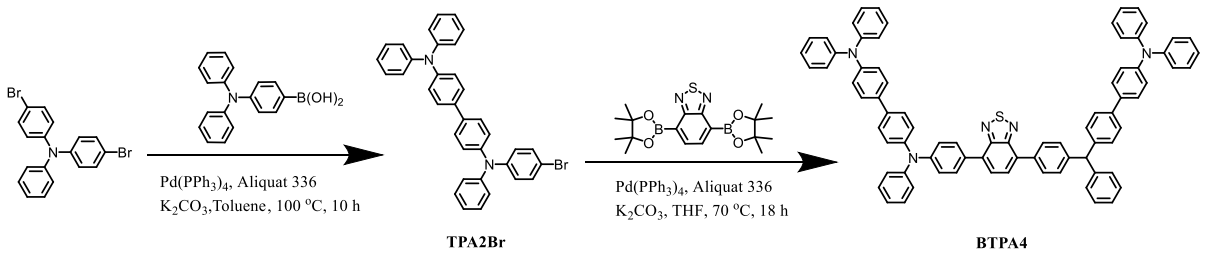

Scheme S2. Molecular structures and synthetic routes of the BTPA4.

Synthesis of N^4-(4-bromophenyl)-N^4, $N^{4'}$, $N^{4'}$-triphenyl-[1,1'-biphenyl]-4,4'-diamine (TPA2Br)

At room temperature, 4-bromo-N-(4-bromophenyl)-N-phenylaniline (2.0 g，4.96 mmol) and (4-(diphenylamino)phenyl)boronic acid (1.2 g，4.13 mmol) were added to a 250 mL three-necked flask and dissolved in 50 mL of toluene. The mixture was stirred for 30 min under an argon atmosphere, then 12.40 mL of a 2 mol/L aqueous solution of K_2CO_3, 8 drops of Aliquat 336 and 0.05 g of Pd $(PPh_3)_4$ were added. The temperature was raised to 100°C and the reaction was stirred for 10 h. After the reaction was completed, the mixture was cooled to room temperature, the solvent was removed by vacuum distillation, and the product was purified by column chromatography (DCM/nH = 1:5 v/v) to obtain a white powder solid (1.00 g, yield 42.6%). ^{1}H NMR (400 MHz, DMSO-d_6) δ 7.59 - 7.53 (m, 4H), 7.45 (d, J = 8.8 Hz, 2H), 7.33 (q, J = 8.1 Hz, 6H), 7.10 - 6.99 (m, 13H), 6.94 (d, J = 8.8 Hz, 2H).

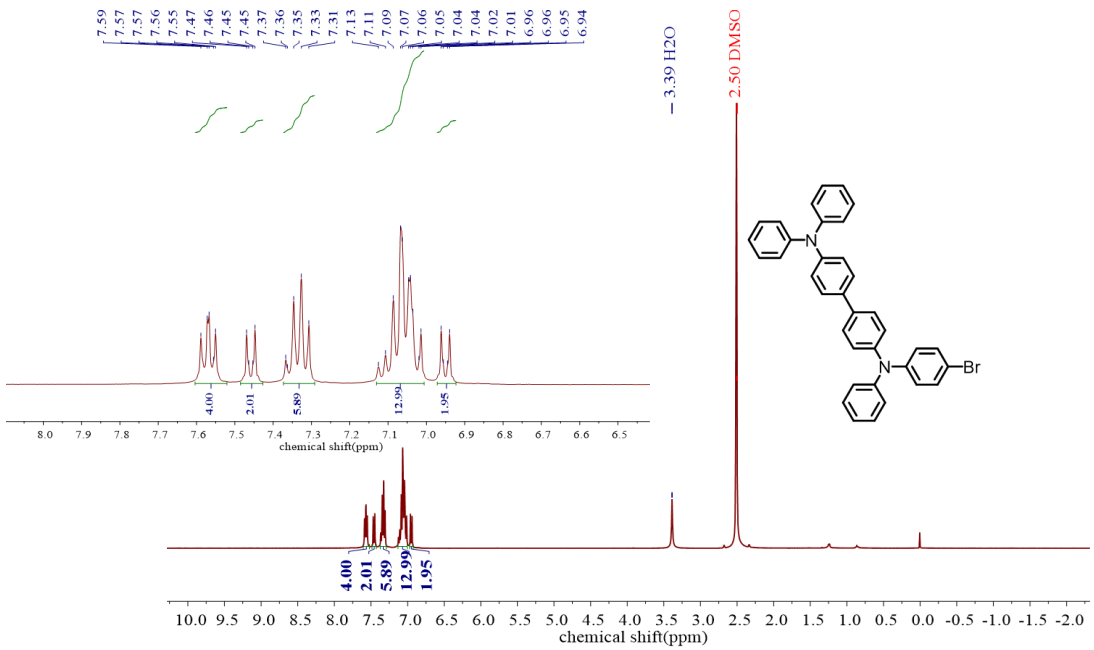

Figure S6. ^{1}H NMR spectrum of TPA2Br in DMSO-d_6.

Synthesis of N^4-(4-(7-(4-((4'-(diphenylamino)-[1,1'-biphenyl]-4-yl) (phenyl) methyl) phenyl) benzo[c] [1,2,5] thiadiazol-4-yl) phenyl)-N^4, $N^{4'}$, $N^{4'}$-triphenyl-[1,1'-biphenyl]-4,4'-diamine (BTPA4)

At room temperature, TPA2Br (0.81 g，1.43 mmol) and 4,7-bis(4,4,5,5-tetramethyl-1,3,2-dioxaborolan-2-yl)benzo[c][1,2,5]thiadiazole (0.24 g，0.62 mmol) were added to a 250 mL three-necked flask and dissolved in 30 mL of THF. The mixture was stirred for 30 min under an argon atmosphere, then 2.17 mL of a 2 mol/L aqueous solution of K_2CO_3, 8 drops of Aliquat 336 and 0.05 g of Pd $(PPh_3)_4$ were added. The temperature was raised to 70°C and the reaction was stirred for 18 h. After the reaction was completed, the mixture was cooled to room temperature, the solvent was removed by vacuum distillation, and the product was purified by column chromatography (DCM/nH = 1:4 v/v) to obtain a red powder solid (0.35 g, yield 50.8%). ^{1}H NMR (400 MHz, Methylene Chloride-d_2) δ 7.97 (d, J = 8.2 Hz, 4H), 7.81 (s, 2H), 7.54 (s, 8H), 7.33 (td, J = 24.5, 23.4, 11.7 Hz, 26H), 7.18-6.96 (m, 16H). ^{13}C NMR (600 MHz, Methylene Chloride-d_2) δ 154.19, 132.01, 129.99,

129.22, 127.35, 127.23, 124.77, 123.99, 123.54, 123.01, 53.03.δ 154.18, 132.01, 127.36, 124.78, 123.98, 53.94, 53.67, 53.40, 53.13, 52.86. HRMS (APCI): m/z, $[M+H]^+$ calcd for $C_{78}H_{56}N_6S$: 1109.43599, found: 1109.43557.

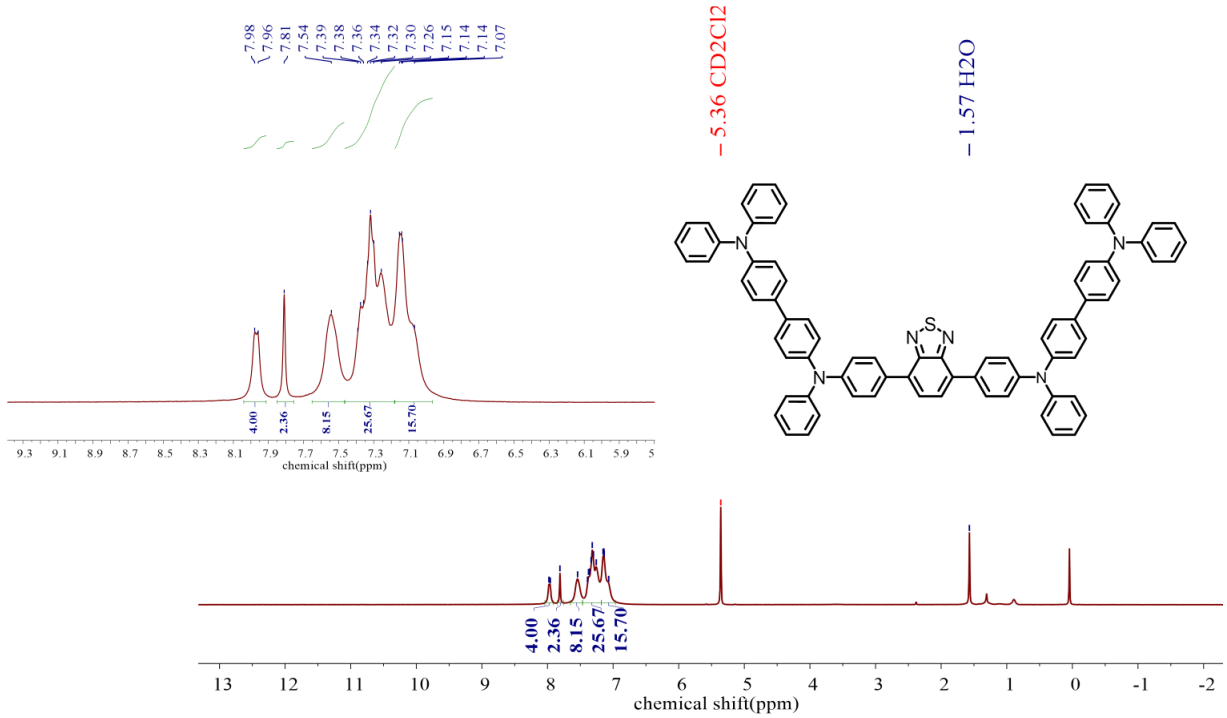

Figure S7. ^{1}H NMR spectrum of BTPA4 in Methylene Chloride-d_2.

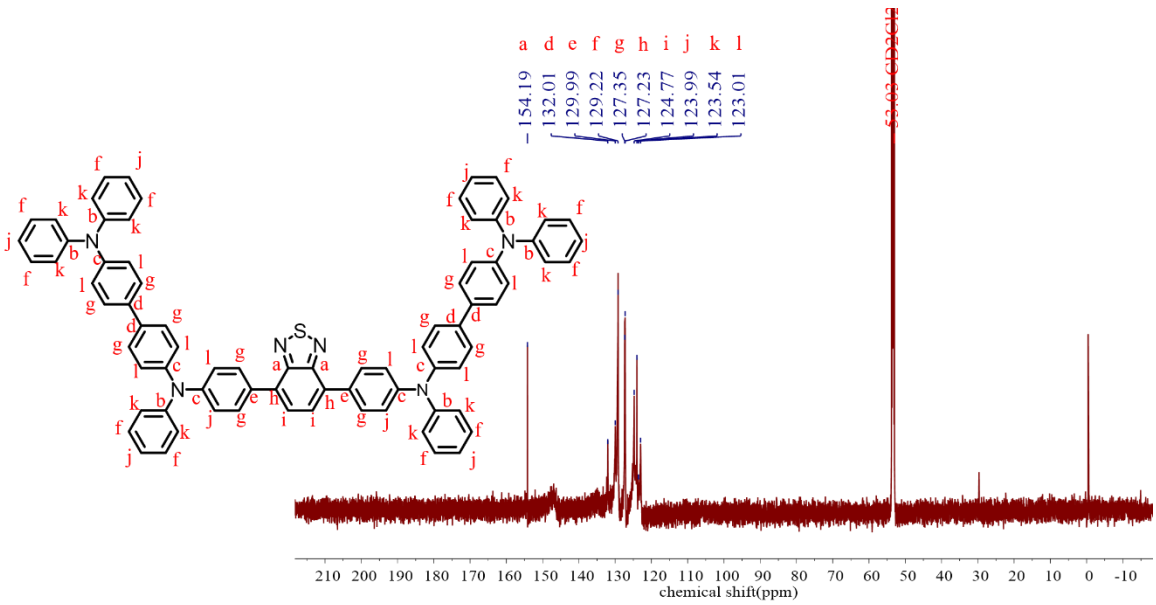

Figure S8. ^{13}C NMR spectrum of BTPA4 in Methylene Chloride-d_2.

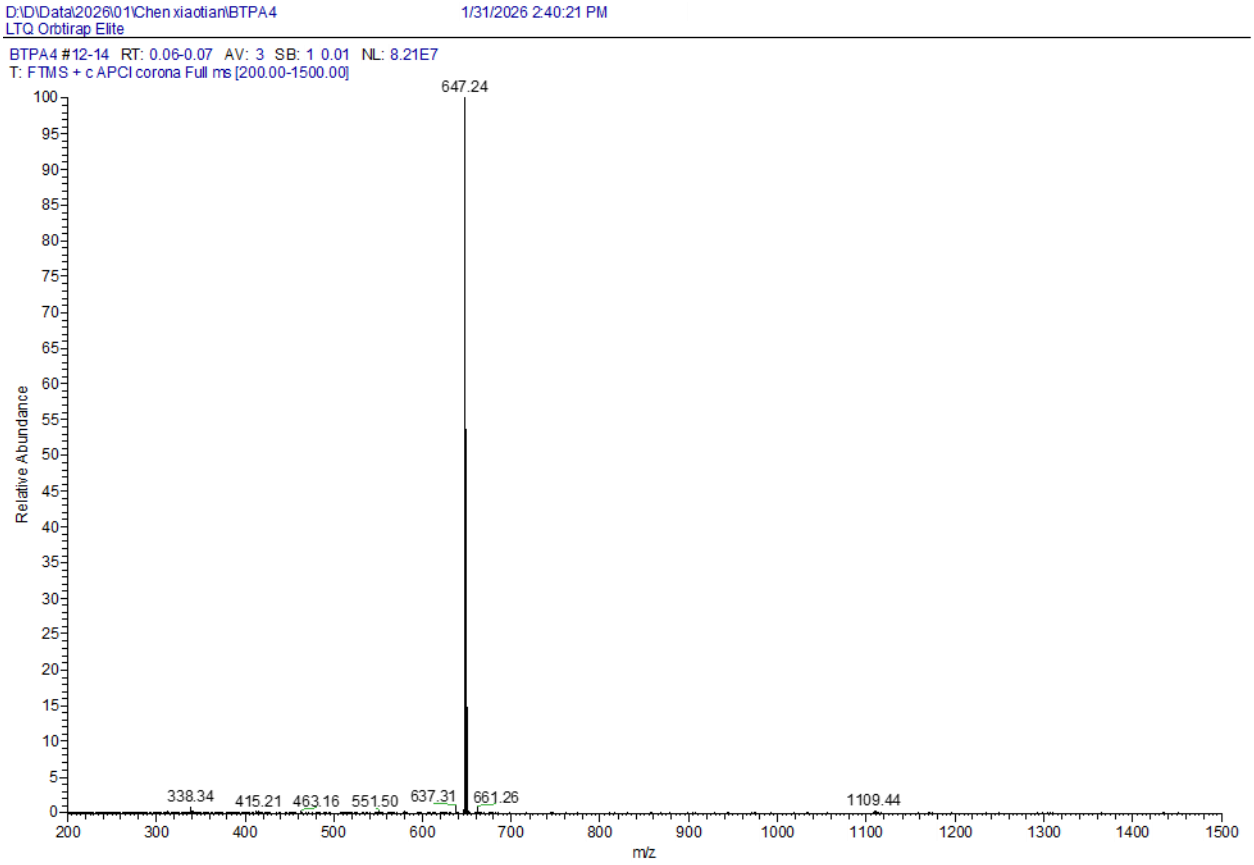

Figure S9. HRMS spectrum of the BTPA4(full-range).

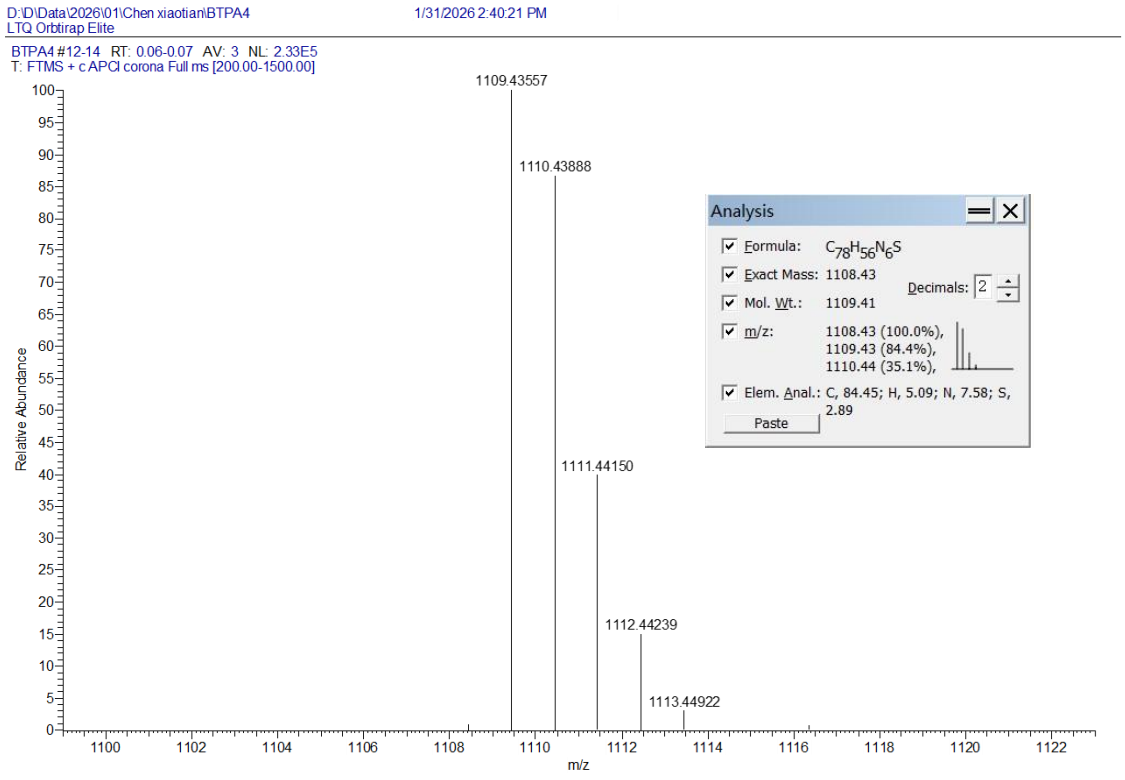

Figure S10. HRMS spectrum of the BTPA4.

Fragmentation assignment for BTPA4: The full-range HRMS spectrum of BTPA4 (Figure S9) shows the most abundant peak at m/z ≈ 647. This fragment is assigned to the cleavage of a labile C–N bond between the triphenylamine-containing arm and the benzothiadiazole core, forming a stable conjugated fragment. The molecular ion peak $[M+H]^+$ (calculated for BTPA4, ~1109) is clearly detectable with a mass error of < 3 ppm (Figure S10), verifying the molecular formula.

S2 Theoretical calculation

CzPyPPI and BTPA4 first performs geometric optimization at the B3LYP/6-31g(d,p) level, followed by calculation at optimized stationary points. Natural transfer orbit (NTO) calculated using PBE0/6-31g(d,p) method. The above calculations were performed in the *Gaussian 09W* package. Using *Multifwn* software to analyze the electron wave function of NTOs, and visualization using Gaussian View program. Based on the theoretical level of B3LYP/G TZVP, the spin-orbit coupling (SOC) matrix elements were analyzed through the *ORCA* 5.0.3 package.

Table S1 The NTO and excited state analysis of CzPyPPI and BTPA4.

	Hole		Particle
CzPyPPI	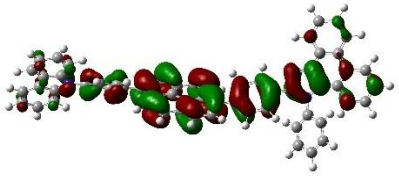	$S_0 \xrightarrow{97.96\%} S_1$ (f=2.0946) Overlap 80.53% LE	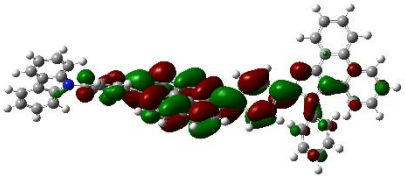
	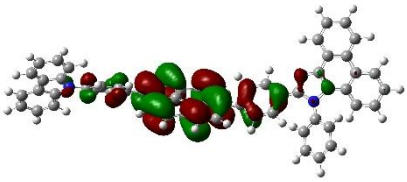	$S_0 \xrightarrow{96.35\%} T_1$ Overlap 87.71% LE	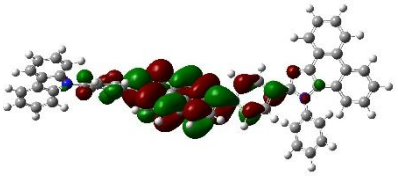
	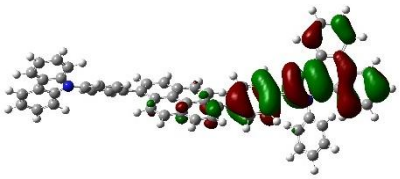	$S_0 \xrightarrow{81.17\%} T_2$ Overlap 78.95% LE	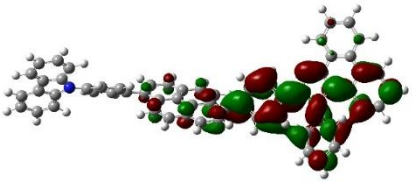
	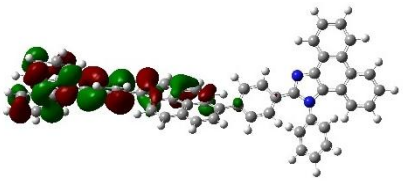	$S_0 \xrightarrow{59.17\%} T_3$ Overlap 69.84% HLCT	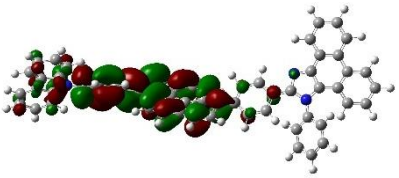
BTPA4	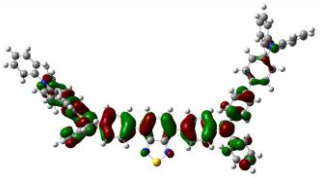	$S_0 \xrightarrow{99.40\%} S_1$ (f=0.5745) Overlap 46.23% HLCT	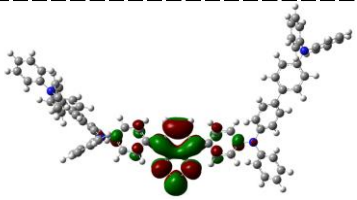
		$S_0 \xrightarrow{99.62\%} T_1$ Overlap 78.55% LE	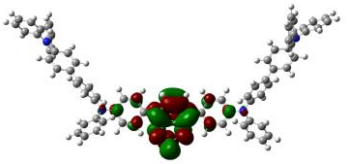
	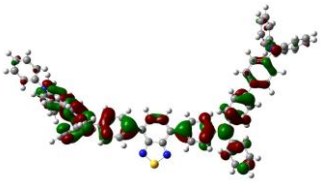	$S_0 \xrightarrow{95.29\%} T_2$ Overlap 41.37% HLCT	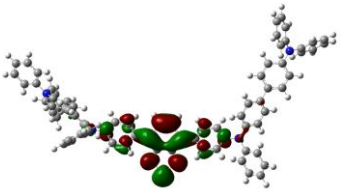
	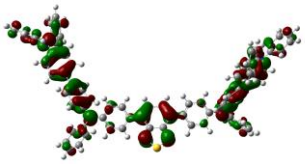	$S_0 \xrightarrow{89.89\%} T_3$ Overlap 55.06% HLCT	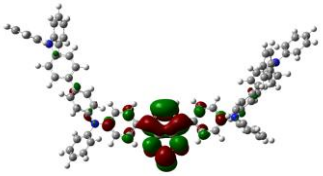

Table S2 SOC constants between the S_1 states and triplet excited states (T_1-T_3).

Compund	$\langle S_1\|\hat{H}_{soc}\|T_1\rangle$ (cm^{-1})	$\langle S_1\|\hat{H}_{soc}\|T_2\rangle$ (cm^{-1})	$\langle S_1\|\hat{H}_{soc}\|T_3\rangle$ (cm^{-1})
CzPyPPI	0.042	0.236	0.164
BTPA4	0.116	0.233	0.201

S3 Photophysical properties

Ultraviolet-visible (UV-Vis) absorption spectra were measured on a Shimadzu UV-3600 UV-Vis-NIR spectrophotometer. Photoluminescence (PL) spectra were measured using a Shimadzu RF-5301PC spectrometer. Transient PL decay characteristics were recorded on Edinburgh FLS1000 spectrometer. The PL quantum yields were determined on a Horiba JY FL-3 spectrometer equipped with a calibrated integrating sphere. The excitation wavelengths for testing are 340 nm (CzPyPPI) and 405 nm (BTPA4), respectively.

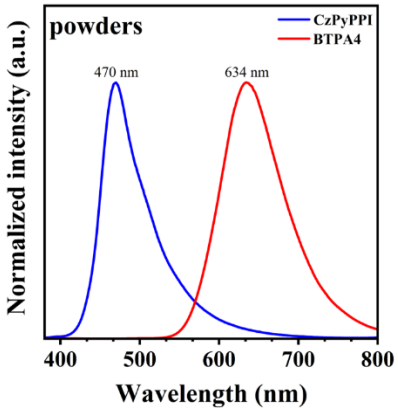

Figure S11. Normalized PL spectra of the solid powders of CzPyPPI and BTPA4.

Preparation of neat and doped films for photophysical measurements

The neat and doped films for photophysical characterization (PLQY and fluorescence lifetime) were deposited on quartz substrates by vacuum thermal evaporation. The deposition was carried out under a base pressure of $< 4\times10^{-4}$ Pa. The quartz substrates were used as received without further cleaning. The evaporation rate was approximately at 1-2 Å/s, and the film thickness was controlled to be 20 nm. All samples were measured under ambient conditions immediately after deposition.

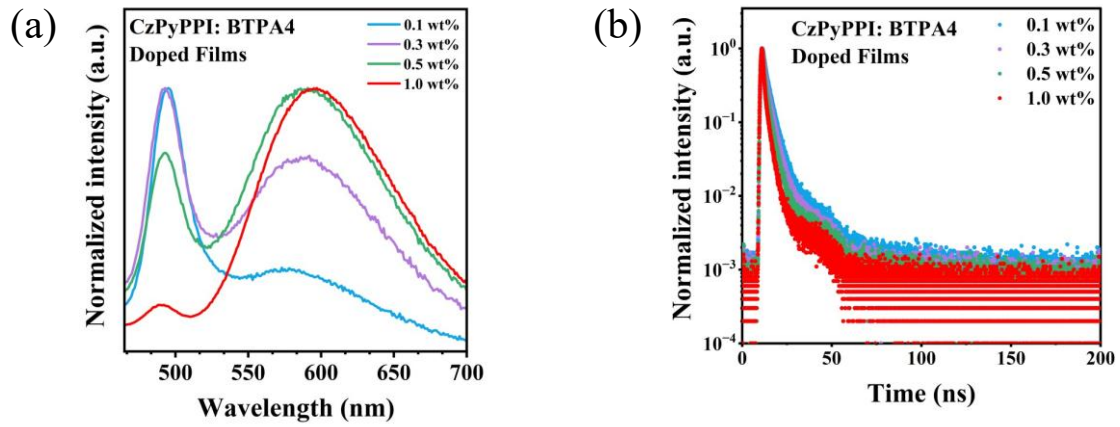

Figure S12 (a) Normalized PL spectra of the CzPyPPI: BTPA4 doped films and (b)The transient decay curves of CzPyPPI and BTPA4 in doped films.

Table S3 Photophysical properties of the CzPyPPI: BTPA4 doped films.

CzPyPPI: BTPA4 X wt% films	λ_{PL} (nm)	CIE(x, y)	PLQY (%)	τ (s^{-1})	k_r (s^{-1})
X =0.1 wt%	495/581	(0.303, 0.418)	83.8	5.92	1.42×10^{8}
X =0.3 wt%	493/591	(0.388, 0.423)	93.1	2.49	3.74×10^{8}
X =0.5 wt%	493/591	(0.434, 0.429)	90.7	3.75	2.42×10^{8}
X =1.0 wt%	493/597	(0.504, 0.431)	95.8	2.96	3.23×10^{8}

Radiative transition rate (k_r) can be calculated by the following formula:

$$k_r = \frac{PLQY\ (\%)}{\tau\ (ns)}\ (10^7\ s^{-1}) \qquad (Eq.S1)$$

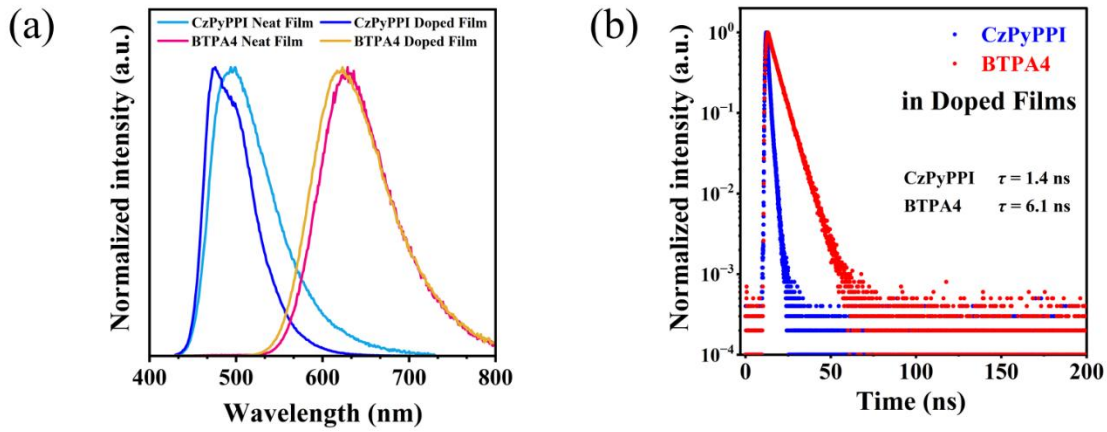

Figure S13 (a) Normalized PL spectra of the neat/doped films of CzPyPPI and BTPA4. (b) The transient decay curves of CBP: 10 wt% CzPyPPI and CBP: 10 wt% BTPA4 doped films.

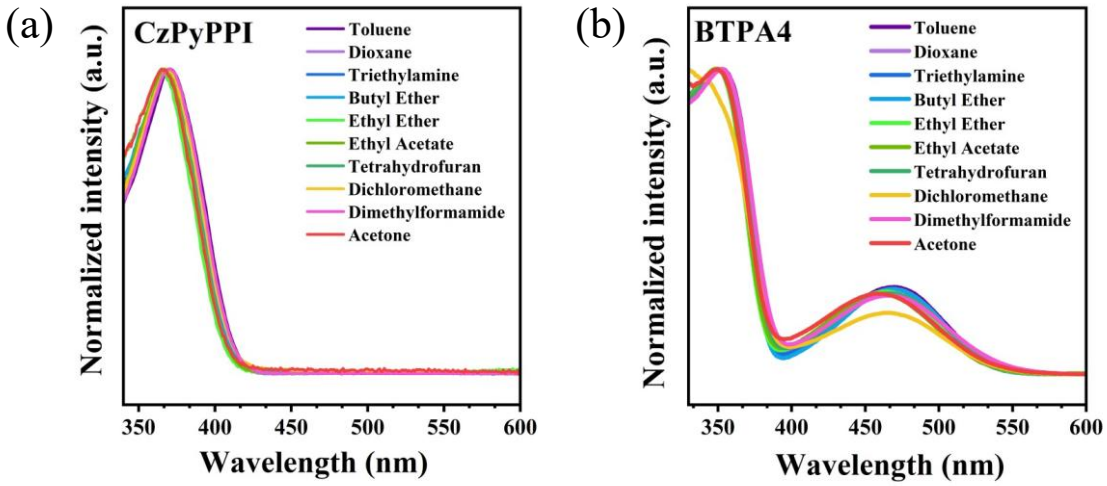

Figure S14 Normalized absorption spectra (a) CzPyPPI and (b) BTPA4 in solvents with different polarities.

S4 The Lippert-Mataga model

The Lippert-Mataga model establishes a linear relationship between the polarity of the solvent and the Stokes shift of the solute molecule, thereby enabling the estimation of the change in the molecular dipole moment in the excited state.

$$hc(\nu_a - \nu_f) = hc(\nu_a^0 - \nu_f^0) + \frac{2f(\mu_e - \mu_g)^2}{a^3} \qquad (Eq.S2)$$

This formula can be simplified as:

$$\mu_e = \mu_g + \left[\frac{hca_0^3}{2} \cdot \frac{d(\nu_a - \nu_f)}{df}\right]^{\frac{1}{2}} \qquad (Eq.S3)$$

μ_e is the dipole moment of excited state, μ_g is the dipole moment of ground state, h is the Plank constant, c is the light speed in vacuum, a_0 is the solvent Onsager cavity radius, $\nu_a - \nu_f$ is the Stokes shift, f is the orientational polarizability of solvents, related to the solvent dielectric constant and the solvent refractive index. $\frac{d(\nu_a - \nu_f)}{df}$ can be estimated based on the solvatochromic experiment data. The μ_g and a_0 values of the two molecules were obtained through theoretical calculations, and the μ_e values of the two molecules were calculated using the Eq. S3.

Table S4 The results obtained based on the Lippert-Mataga equation of CzPyPPI and BTPA4.

Compund and solvents		$\frac{d(\nu_a-\nu_f)}{df}$(cm^{-1})	μ_g(D)	a_0^3(10^{-22} cm^3)	μ_e(D)
CzPyPPI	low-polarity solvents	2311	2.92	2.40	10.35
	high-polarity solvents	9345			17.86
BTPA4	low-polarity solvents	1813	1.73	3.59	9.08
	high-polarity solvents	11473			20.94

Table S5 Detailed absorption and emission peaks of CzPyPPI and BTPA4 in different solvents.

Solvents	f	**CzPyPPI**			**BTPA4**		
		λ_a (nm)	λ_f (nm)	ν_a-ν_f (cm^{-1})	λ_a (nm)	λ_f (nm)	ν_a-ν_f (cm^{-1})
Toluene	0.014	370	450	4805	470	609	4856
Dioxane	0.021	370	450	4805	463	624	5573
Triethylamine	0.048	367	446	4826	469	588	4315
Butyl ether	0.096	367	456	5026	469	591	4401
Ethyl Ether	0.167	366	450	5100	465	606	5004
Ethyl acetate	0.200	367	452	5124	462	639	5996
Tetrahydrofuran	0.210	370	456	5097	466	636	5736
Dichloromethane	0.217	369	456	5170	466	665	6422
Dimethyl formamide	0.276	371	468	5587	467	690	6920
Acetone	0.284	365	468	6030	458	665	6796

S5 Electrochemical properties

5 mL of 5×10^{-4} M super-dry DCM solutions of **CzPyPPI** and **BTPA4** were separately prepared. Cyclic voltammetry (CV) measurements were carried out on a VMP300 electrochemical workstation (Bio-Logic). A three-electrode system was employed, consisting of an Ag/AgCl reference electrode, a Pt counter electrode, and a glassy carbon working electrode. A 0.1 M DCM solution of tetra-n-butylammonium hexafluorophosphate served as the supporting electrolyte, with ferrocene as the internal standard.

$$E_g = \frac{1240}{\lambda_{onest}} \quad \text{(Eq. S4)}$$

$$HOMO = -(E_{onset}^{ox} + 4.8)\ eV \quad \text{(Eq. S5)}$$

$$LUMO = HOMO + E_g \quad \text{(Eq. S6)}$$

Herein, λ_{onset} denotes the onset absorption wavelength in the UV-visible absorption spectrum, and E_{onset}^{ox} refers to the onset oxidation potential obtained from the CV curve.

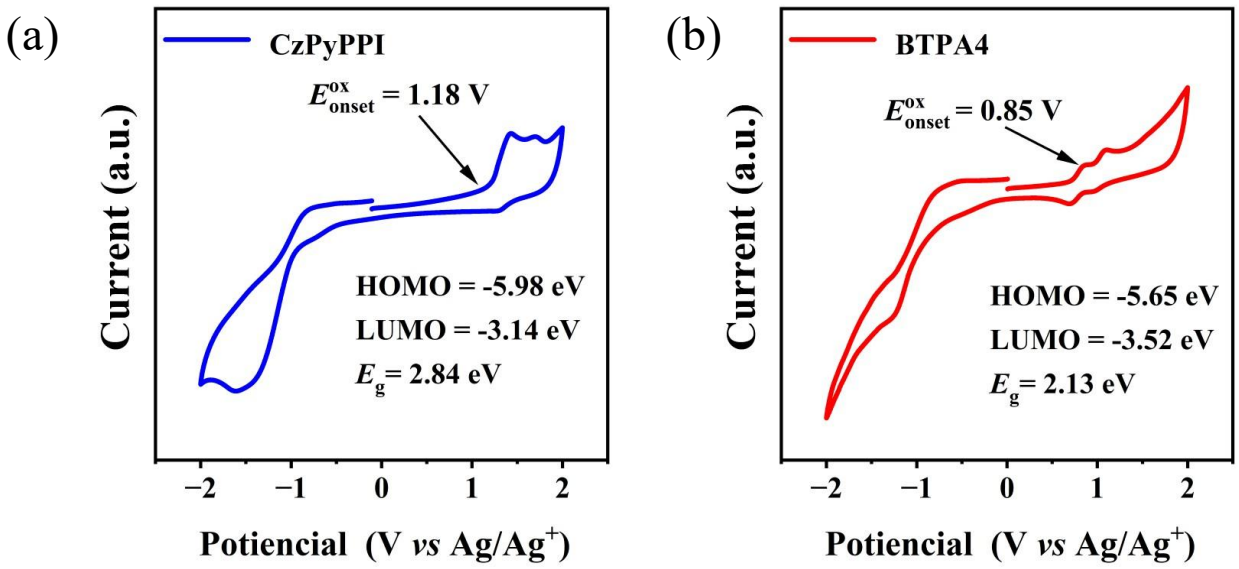

Figure S15. Cyclic voltammograms (CV) of (a) CzPyPPI and (b) BTPA4.

S6 Thermal properties

Thermogravimetric analyses (TGA) were conducted with a TA thermal analyzer (NETZSCH TG 209F1 Libra) under N_2 atmosphere from 20 to 800 ℃ with a heating rate of 20 ℃ min^{-1}. Differential scanning calorimetry (DSC) was performed using a DSC204F1 under N_2 atmosphere from 20 to 500 ℃ with a heating rate of 20 ℃ min^{-1}.

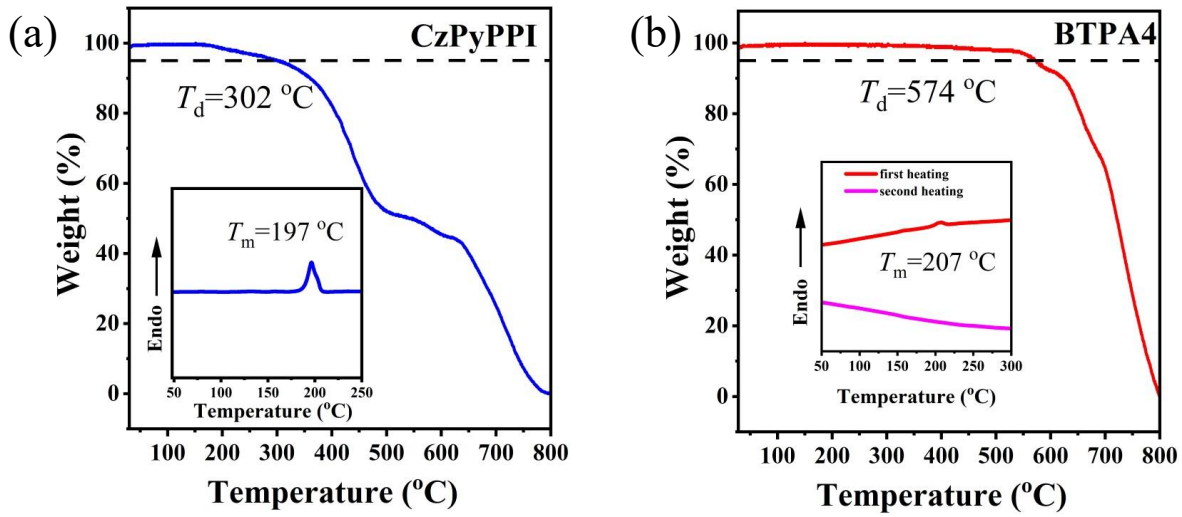

Figure S16. Thermogravimetric analysis and differential scanning calorimetry spectra of (c) CzPyPPI and (d) BTPA4.

S7 Carrier mobility

Electron-only devices (EODs): ITO/ TmPyPB (10 nm)/CzPyPPI(20 nm)/ TmPyPB (10 nm)/ LiF (1 nm)/Al (130 nm). Hole-only devices (HODs): ITO/ TAPC (10 nm)/CzPyPPI(20 nm)/ TAPC (10 nm)/ LiF (1 nm)/Al (130 nm).

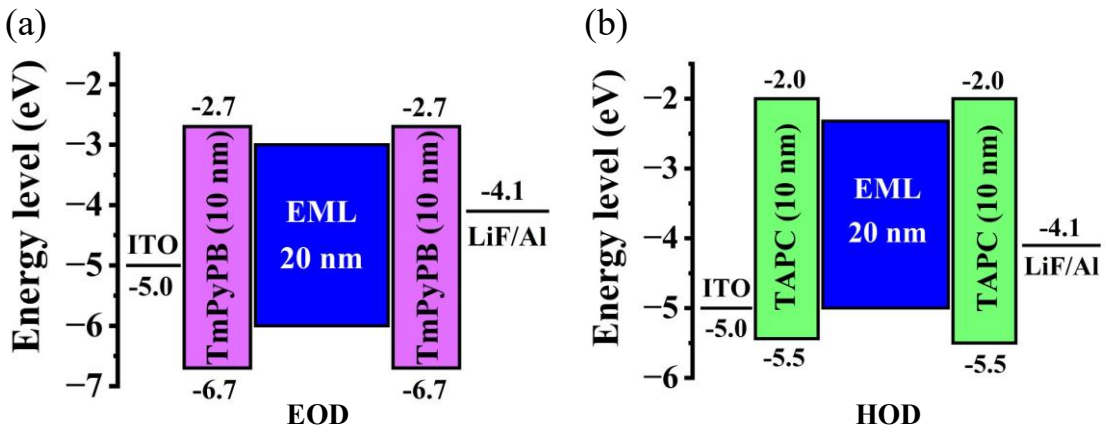

Figure S17. The architecture of (a) electron-only devices; (b) hole-only device.

The space-charge-limited current (SCLC) characteristics can be described by the following Mott-Gurney equation:

$$J = \frac{9}{8}\varepsilon_0\varepsilon_r\frac{V^2}{L^3}\mu_0 \exp\left(0.891\gamma\sqrt{\frac{V}{L}}\right) \quad \text{(Eq. S7)}$$

Here, J represents the current density, free-space permittivity ε_0=8.85 × 10^{-14} C V^{-1} cm^{-1}, and in organic semiconductors， relative dielectric constant ε_r usually assumed to be 3.0, L is the thickness of EML (20 nm)， γ is the Poole-Frenkel factor and μ_0 is the zero-field mobility. Based on the J-V curve fitting, the values of γ and μ_0 can be obtained. And the carrier mobility (μ) can be expressed via the Poole-Frenkel formula:

$$\mu = \mu_0 \exp\left(\gamma\sqrt{E}\right) \quad \text{(Eq. S8)}$$

Here, E represents the electric field strength, which can be obtained by V/L. Finally, the μ-$\sqrt{E}$ curve can be plotted as follows.

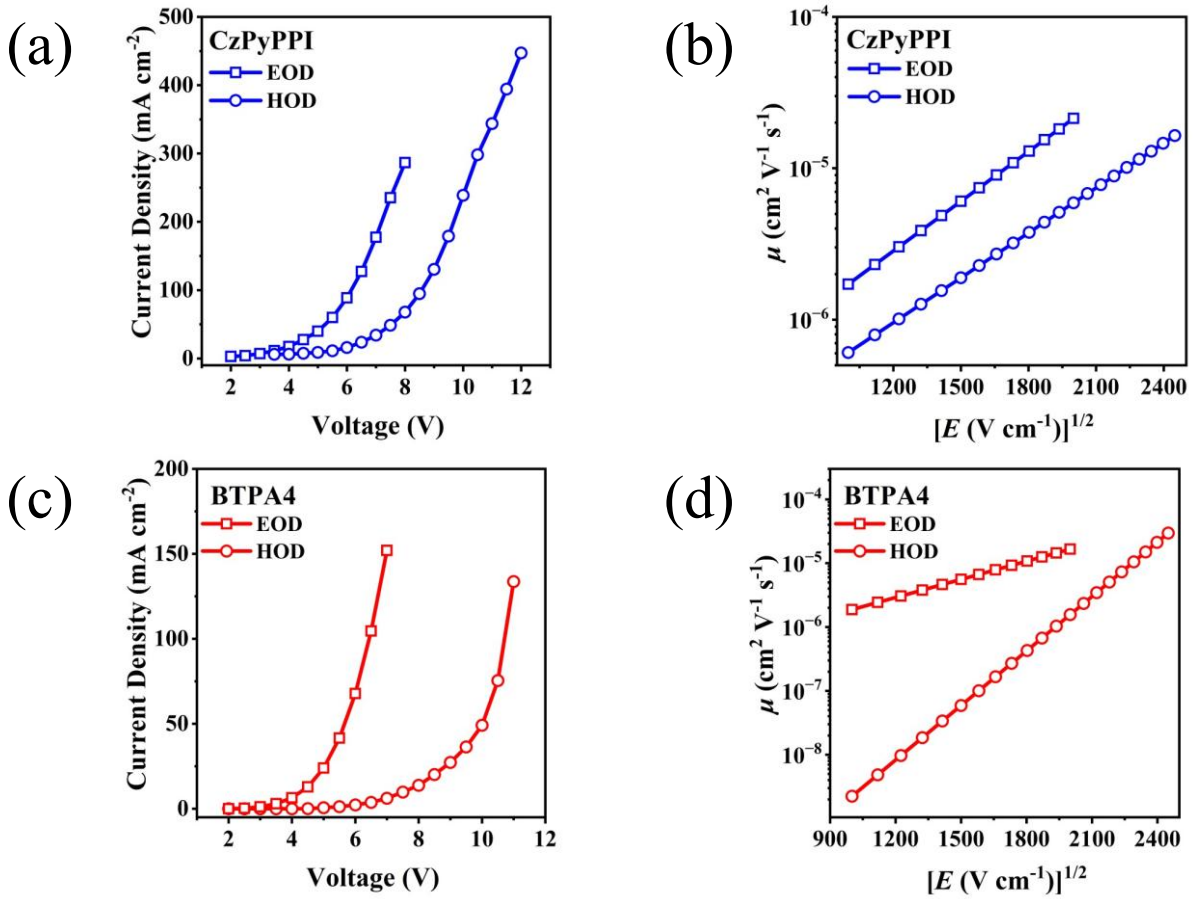

Figure S18. Current Density-Voltage (J-V) curve of (a)CzPyPPI, (c)BTPA4; Carrier mobilities in single carrier devices of (b)CzPyPPI, (d)BTPA4.

Table S6 The average electron mobility (μ_e) and average hole mobility (μ_h) of CzPyPPI and BTPA4.

Compound	EOD μ_e (cm^2 V^{-1} s^{-1})	HOD μ_h (cm^2 V^{-1} s^{-1})
CzPyPPI	5.89×10^{-6}	9.01×10^{-6}
BTPA4	7.65×10^{-6}	4.71×10^{-6}

S8 Devices performance

The Indium Tin Oxide (ITO) glass substrate was successively treated with 5% Decon cleaning agent, pure water and isopropyl alcohol for 3 minutes under ultrasonic conditions. Then it was placed in an oven for drying overnight. After drying, the layers were molecularly deposited onto the ITO substrate surface in the Fangsheng FS450 S-16 under a vacuum pressure lower than 4×10^{-4} Pa. Among them, the deposition rate of LiF was 0.1 Å/s, that of Al was 2.0 Å/s, and the deposition rates of the other organic layers were 0.5-1.0 Å/s. Device performance were measured using a TOPCON-SRUL1R and a Keithley 2400 source. Including *J-V-L* properties, external quantum efficiency, and electroluminescence spectra and their CIE coordinate. The tested emitting area is 0.09 cm^2.

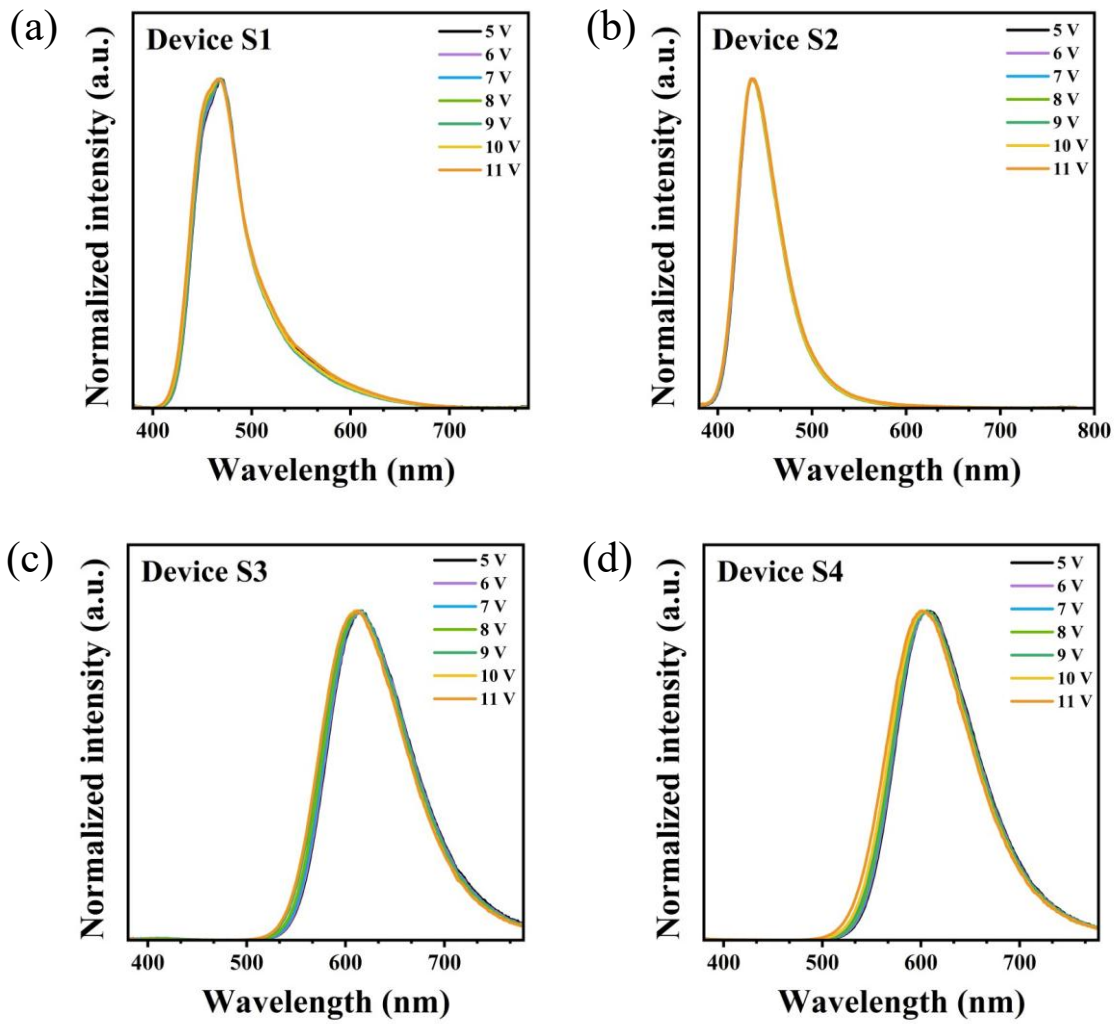

Figure S19. Normalized EL spectra performance of blue and orange OLED (a) Device S1; (b) Device S2; (c) Device S3; (d) Device S4.

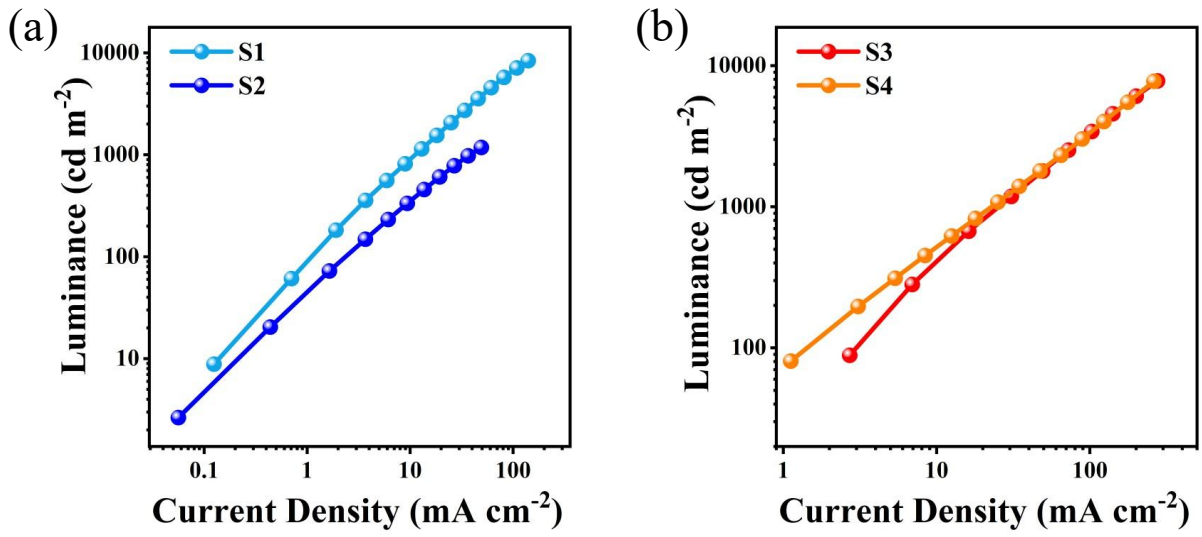

Figure S20. The luminance-current density curves of (a) blue OLED; (b) orange OLED.

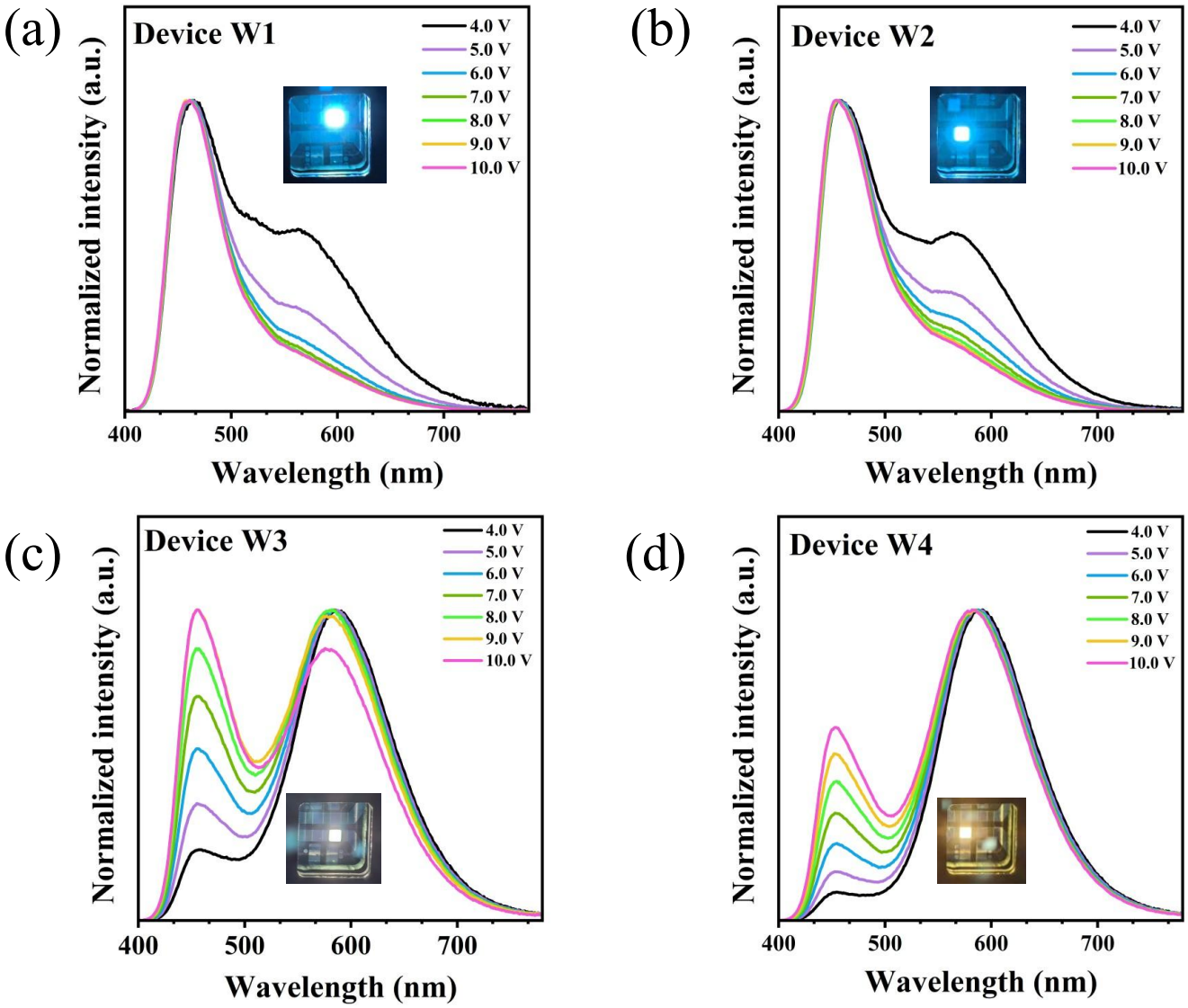

Figure S21. Normalized EL spectra performance of WOLED (a) 0.1 wt%; (b) 0.3 wt%; (c) 0.5 wt%; (d) 1.0 wt%. inset: photo of each device at 10 V.

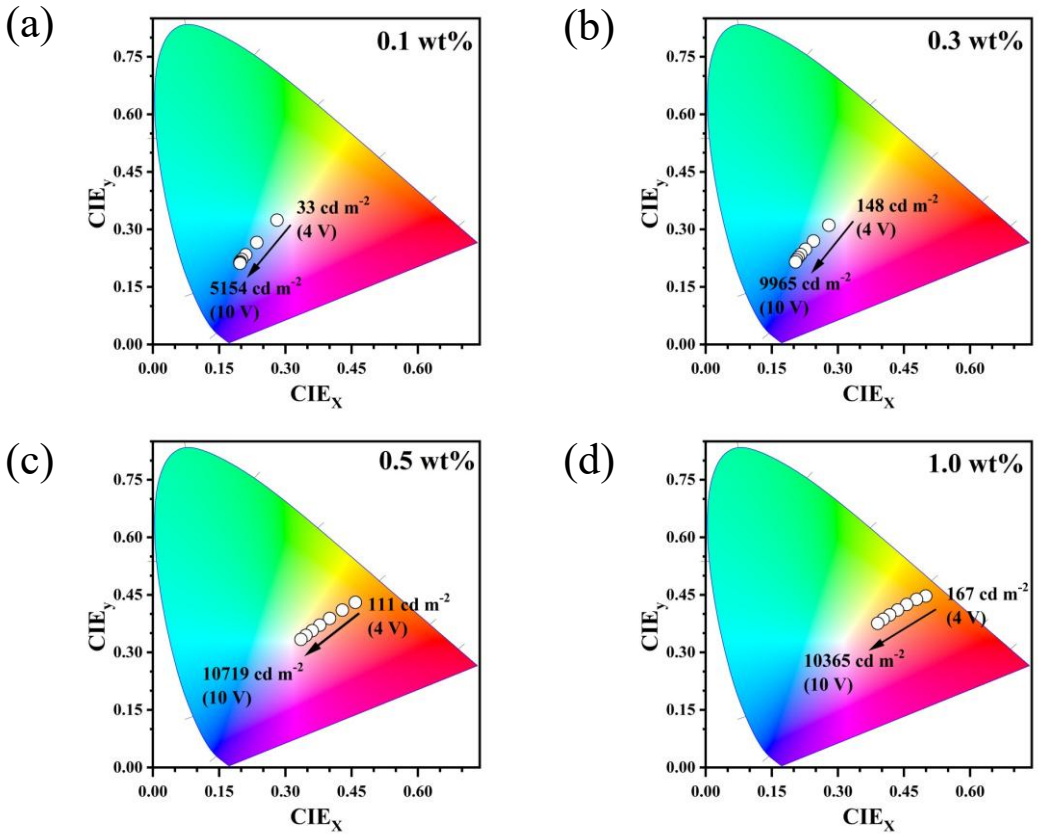

Figure S22. CIE coordinates with luminance and voltage of WOLEDs (a) 0.1 wt%; (b) 0.3 wt%; (c) 0.5 wt%; (d) 1.0 wt%.

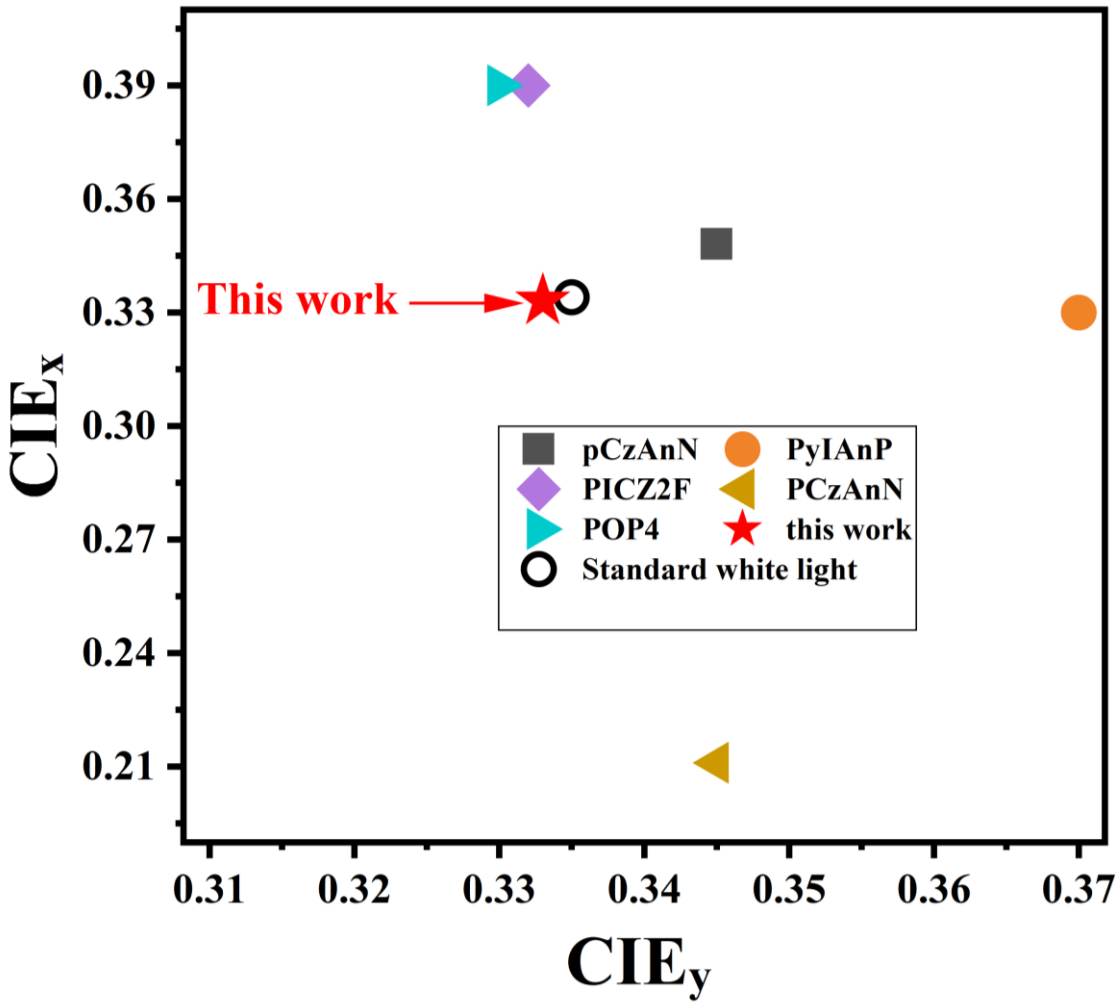

Figure S23. The summary of CIE coordinates of some use of HLCT molecules as host for the EML in all-fluorescence WOLEDs.

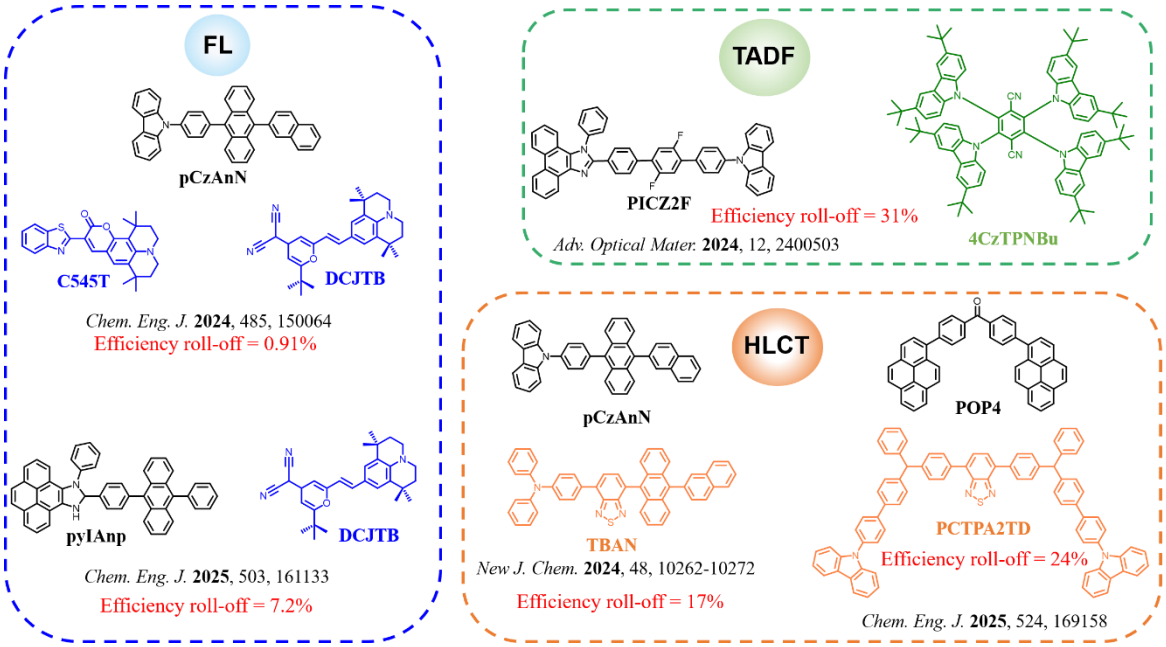

Figure S24. Molecular structures of HLCT materials used as the host of the WOLED and molecular structures of FL, TADF and HLCT materials used as the guest of the WOLED.

References

[1] Y.-S. Lee, H. Nam, Y.-N. Sang, W.-P. Hong, W.-S. Han and T. Kim, *Chem. Eng. J*, 2025, **521**, 166658.

[2] J. Yang, Q, Guo, J. Wang, Z. Ren, J, *Chen, Adv. Opt Mater.*, 2018, **6**, 1800342.

[3] L. Zou, S. Guo, H. Lv, F. Chen, L. Wei, Y. Gong, Y. Liu, C. Wei, *Dyes Pigm.*, 2022, **198**, 109958.

[4] H. Zhang, B. Zhang, Y. Zhang, Z. Xu, H. Wu, P. Yin, Z. Wang, Z. Zhao, D. Ma, and B. Z. Tang, *Adv. Funct Mater.*, 2020, **30**, 2002323.

[5] H. Ma, X. Niu, W. Qu, Z. Feng, T. Ma,Y. Liu and S. Zhu. *J. Mater. Chem. C.*, 2025, **13**, 16998.

[6] L. Zhang, C. Ma, X. Wang, Y. Zhou, J. Song, M. Sun, Q. Sun, S. T. Zhang, W. Yang and S. Xue. *Chem. Sci*., 2025, **16**, 14478.